Sensors & Diagnostics

PAPER

View Article Online
View Journal

Cite this: DOI: 10.1039/d5sd00210a

Low-cost printed circuit board (PCB) electrochemical biosensors for rapid and label-free detection of *Streptococcus pneumoniae*

Vincent Vezza,[a] Veerappan Mani,[a] Niamh Docherty,[a] Adrian Butterworth,[a] David Alcorn,[b] Paul A. Hoskisson[c] and Damion Corrigan*[a]

Severe sepsis presents a critical healthcare challenge where rapid pathogen identification is vital for timely intervention. Current diagnostic methods, however, remain inadequate, often delaying targeted treatment. Using readily available printed circuit board (PCB) electrodes, we address this need by developing a low-cost electrochemical DNA biosensor for rapid detection of *Streptococcus pneumoniae* using the *lytA* gene as a biomarker. Through systematic evaluation of commercial and custom PCB designs (P1–P4), gold-plated PCB P4 was found as the optimal platform, demonstrating sensitive detection of *lytA* sequences (20 bp at 4.50 pM limit of detection in buffer) and clinically relevant 235 bp polymerase chain reaction (PCR) amplicons in 100% human serum (1.0–100 pM) within 15 min at room temperature using electrochemical impedance spectroscopy. The performance of the biosensor originates from the optimized electrode geometry, surface properties, and robust self-assembled monolayer functionalization, enabling specific recognition of bacterial DNA without sample pretreatment. This work establishes PCB-based biosensors as a promising solution for point-of-care sepsis diagnostics, offering significant advantages in speed, cost, and operational simplicity compared to conventional methods.

Received 19th November 2025,
Accepted 29th January 2026

DOI: 10.1039/d5sd00210a

rsc.li/sensors

1. Introduction

Severe sepsis is a life-threatening medical emergency that provides a significant challenge to clinicians and health care systems.[1] The UK sepsis trust database indicates that sepsis is responsible for 11 million deaths globally each year and 48 000 sepsis related deaths each year in the UK.[2] Sepsis is an extremely challenging illness to diagnose as there is often a multitude of signs, symptoms and measurements that can occur and can be attributed to many other serious or benign medical conditions.[3] Among the various pathogens responsible for sepsis, *Streptococcus pneumoniae* infection is commonly fatal particularly in cases of community-acquired respiratory infections, highlighting the urgent need for rapid and specific diagnostic tools.[4–6] There is a growing demand for a low-cost, rapid point-of-care (PoC) diagnostic device capable of detecting *Streptococcus pneumoniae*, not only in hospitals but also in community screening, primary care, and home healthcare settings.[7]

Phenotypic identification, genotypic identification, and mass spectrometry are the three key methods used for this purpose; the main issue with such methodologies is that they can take hours to days to result.[8–10] Phenotypic identification, the current gold standard, relies on culturing blood samples to observe bacterial growth, followed by biochemical testing which typically requires more than 72 hours. Genotypic identification relies on DNA or RNA analysis through techniques like 16S/23S ribosomal DNA sequencing and amplified ribosomal DNA restriction analysis (ARDRA), but they are limited by time consumption, the need for specialized equipment and expertise, and reduced effectiveness in distinguishing closely related strains. Matrix-assisted laser desorption/ionization time-of-flight mass spectrometry (MALDI-TOF MS) identifies pathogens by analysing their protein mass spectra through laser desorption and time-of-flight measurement, offering rapid, cost-effective detection but is limited by the need for prior colony cultivation (24–48 hours), dependence on reference spectra, and database availability.[10] Notably, all these methods are lab-centric and not suitable for PoC use. The pneumococcal urinary antigen test is the only currently available PoC device that can provide a time to result upon sample application in 15 min; however, it requires temperature equilibration of

[a] University of Strathclyde, Centre for Advanced Measurement Science and Health Translation, Pure and Applied Chemistry, Thomas Graham Building, 295 Cathedral St, Glasgow G1 1XL, UK. E-mail: damion.corrigan@strath.ac.uk
[b] Department of Anaesthesia, Royal Alexandra Hospital, Corsebar Rd, Paisley, PA2 9PN, UK
[c] Strathclyde Institute of Pharmacy and Biomedical Sciences, 161 Cathedral St, Glasgow G4 0RE, UK

samples and reagents and involves multiple manual steps, and its generalizability can be uncertain.[11,12] These drawbacks highlight the need for the development of better PoC devices.

Electrochemical biosensors are a promising solution, offering potential for miniaturization, low cost, and rapid results.[13,14] Specifically, printed circuit board (PCB) electrodes are a compelling platform because they have significant advantages, including high customizability through modern design software, established manufacturing processes for rapid, precise, and low-cost mass production, and a variety of available metal plating finishes.[15,16] Increased electrode numbers can be manufactured on smaller surfaces resulting in higher sample sizes within smaller time intervals. Due to the maturation of PCB systems and their extensive incorporation in modern electronic devices, they can be easily integrated into electrochemical readers. They can have additional electronics easily incorporated onto or conjoined to the electrode system of the end goal device. PCB biosensors have been reported in the literature with a wide range of research applications undertaken.[17] However, a label-free PCB-based DNA sensor for the direct detection of *S. pneumoniae* in clinically relevant matrices like human serum has not been demonstrated.

The main objective of this work is to develop PCB-based low-cost, rapid diagnostic test strips for rapid detection of *Streptococcus pneumoniae*, to tackle existing limitations in sepsis diagnostics. Four different PCBs (P1–P4) have been demonstrated in this work, each having different electrode configurations, sizes, geometries, surface materials, and manufacturing methods (Fig. 1). The four PCB electrodes were not selected to enable direct comparison between identical surfaces, but rather to represent distinct and practically relevant PCB manufacturing routes: PCB P1: fully in-house fabricated prototype, PCB P2: commercially fabricated board with in-house gold plating, PCB P3: standard commercial fabrication (bare copper), and PCB P4: commercially fabricated and optimized for biosensing (gold-plated). The aim of the study was to assess how these different fabrication pathways commonly encountered during biosensor development and scale-up influence electrode surface characteristics and biosensing performance. By functionalising PCB electrodes with a DNA probe sequence that specifically binds to a truncated sequence derived from the *S. pneumoniae lytA* gene which encodes the major autolysin *lytA*, a label-free *S. pneumoniae* biosensor platform was developed.[18] Amplification of a 235 bp from the *lytA* gene has been shown to electrochemically distinguish *S. pneumoniae* from similar streptococci.[19] Our investigation shows that PCB P4 biosensor can detect 10 pM levels of *lytA* in buffer. The amplified 235 bp *lytA* was detectable at 1.0 pM in complex human serum with a 15 min time to result at room temperature.

2. Experimental

2.1. Reagents

Deionized (DI) water (resistivity ≥18 MΩ cm), hydrogen peroxide (H_2O_2), phosphate buffered saline tablets (PBS), potassium chloride (KCl), potassium ferricyanide ($K_3[Fe(CN)_6]$), potassium ferrocyanide ($K_4[Fe(CN)_6]$), sulfuric acid (H_2SO_4), tris(2-carboxyethyl)phosphine (TCEP), and 3-mercapto-1-propanol (MCP) were purchased from Sigma. Acid piranha solution was prepared by mixing 18.0 M H_2SO_4 and 30% H_2O_2 in a volume ratio of 3 : 1 (v/v). PBS (pH 7.40) was the buffer used throughout unless otherwise specified. All oligonucleotides (probe, target, and primers) were obtained from Sigma, and their sequences are provided in Table 1.

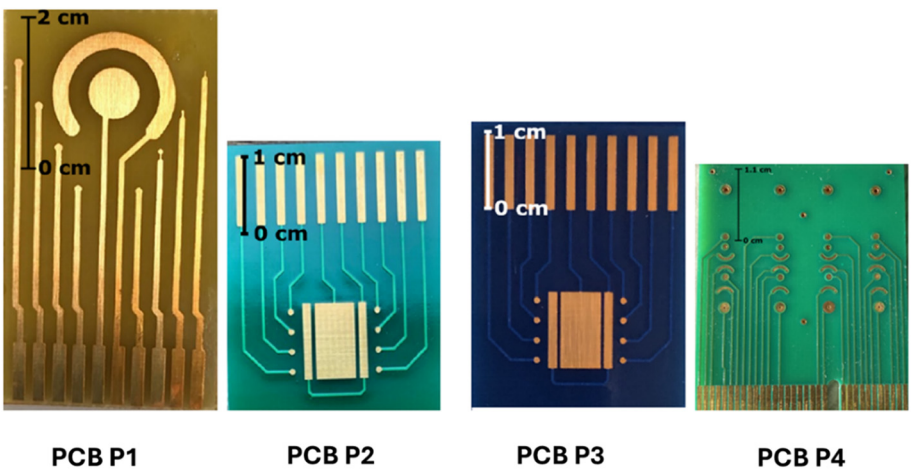

Fig. 1 PCB designs used in the study. PCB P1: initial prototype design. PCB P2: commercially fabricated and hard gold-plated version with an updated layout for improved efficiency and accessory compatibility. PCB P3: commercially fabricated bare copper board with the same layout as P2 but without gold plating. PCB P4: purchased from a PCB biosensor company, BIOTIP Biodevice Technology.

Table 1 List of probes, targes, and primers

Oligonucleotide	Sequence (5′ - 3′)
lytA probe	[ThilC6] [SP18] TGCCGAAAACGCTTGA TACA
lytA target	TGTATCAAGCGTTTTCGGCA
lytA forward primer	TTGGGAACGGTTGCATCATG
lytA reverse primer	TCGTGCGTTTTAATTCCAGCT
blaOXA-1 forward primer	AACAGAAGCATGGCTCGAAA
blaOXA-1 reverse primer	TGGTGTTTTCTATGGCTGAGTT

2.2. Custom PCB electrodes

Four PCB electrodes featuring 4 different designs and geometries are named as PCB P1, PCB P2, PCB P3, and PCB P4. Detailed specifications of all the electrodes are provided in Table S1. All PCB boards used the same electrochemical cell setup for the plating process. Once each board had obtained a gold surface finish, it was cleaned to remove any impurities and contaminants. The details about the cell configuration for electrode plating and cleaning, the plating procedure, and the cleaning procedure are given in the SI (sections S1–S3, Tables S1 & S2, and Fig. S1 & S2). The reference and counter electrode geometries differ between PCB designs as part of an exploratory study into layout efficiency. While these geometric variations can influence absolute electrochemical parameters, all designs were controlled to maintain stable reference potentials and adequate counter electrode competence. The comparative performance assessment focuses on the normalized biosensing response (*i.e.*, the change in impedance or current, not the absolute values) measured under identical assay conditions, ensuring that observed differences are attributable to the overall sensing platform rather than to the reference/counter electrode geometries.

2.3. Fabrication of a DNA biosensor

All experiments used the same protocol for probe functionalisation and a scheme is provided in Fig. 2A. A solution mixture containing 3.0 μM *lytA* probe solution and 15 μM TCEP solution was first prepared. This mixture was applied to the PCB electrode cell surface and incubated overnight at room temperature. PBS washing was then performed to remove any non-specifically bound DNA. The electrode surface was subsequently backfilled with 1.0 mM MCP for 1 h at room temperature, followed by another PBS washing step to eliminate excess materials. This process yielded the final *lytA* PCB biosensors. For a typical electrochemical measurement of *lytA* detection, target concentrations were sequentially incubated on the biosensor electrode surface for 30 min at room temperature. After each incubation, the electrodes were washed with PBS to remove unbound materials before measurement. This cycle was repeated for each concentration. The sequences of the *lytA* primers and probes were adopted from the previous literature.[19] The blaOXA-1 (oxa) primers were designed in-house using the *E. coli* plasmid pEK499 genome sequence, based on methods described in previous studies.[20]

2.4. Polymerase chain reaction (PCR) amplification

PCR amplifications were carried out using a miniPCR mini8 thermal cycler, and the resulting products were analysed using a blueGel electrophoresis system (miniPCR Bio, Cambridge, MA, USA) (Fig. 2B). Quantification of PCR products was performed using a Qubit 4 fluorometer (Thermo Fisher Scientific). The 235 bp *lytA* amplicons were amplified from *S. pneumoniae* genomic DNA TIGR4 [ATCC BAA-334] (LGC Standards, Middlesex, UK), while the oxa amplicons were amplified from *E. coli* plasmid pEK499. Asymmetric PCR was achieved by lowering the concentration of the forward primer, resulting in an unequal amount of forward and reverse segments to hybridize, and thereby producing a higher concentration of single-stranded DNA (ssDNA) target amplicons. Asymmetric digoxigenin (DIG)-labelled amplification followed the same approach but used a DIG PCR mix (Sigma-Aldrich) in place of the standard mix, allowing incorporation of DIG into the amplified sequence. The DIG-labelled target was subsequently detected using a horseradish peroxidase (HRP)-conjugated anti-digoxigenin antibody [HRP.21H8] (Abcam), which binds specifically to the DIG moiety. The bound HRP facilitates the oxidation of 3,3′,5,5′-tetramethylbenzidine (TMB), which can then be electrochemically reduced and quantified *via* chronoamperometry.

2.5. PCR amplicons in PBS

Various types of 235 bp *lytA* PCR amplicons (positive control) and 115 bp oxa PCR amplicons (derived from OXA-48-type ß-lactamase gene; negative control) were utilized in the experiments. The used amplicon types included (1) standard PCR amplicons for *lytA* and oxa, which required preheating at 95 °C for 5 min to denature the double-stranded DNA, (2) asymmetric *lytA* and oxa PCR amplicons, which did not require heat treatment, and (3) asymmetric DIG-labelled *lytA* and oxa PCR amplicons for electrochemical detection *via* antibody recognition. All amplicons were diluted in 1× PBS, and a range of target concentrations was tested. Target incubation was performed for 15 min at room temperature, followed by PBS and 0.05% Tween washing steps prior to measurement. For DIG-labelled PCR amplicons, chronoamperometric detection was carried out by incubating the electrodes with anti-DIG antibodies (diluted 1 : 1000 from stock) for 30 min at room temperature. This was followed by a brief 20 s 1× PBS washing step, after which 10 μL of TMB substrate was added and allowed to react for 20 min. Chronoamperometry was then performed with an applied potential (E_{dc}) of −0.15 V for 2 s.

2.6. PCR amplicons in human serum

PCB P4 was used for all experiments given in this section. Standard *lytA* and oxa PCR amplicons were first denatured

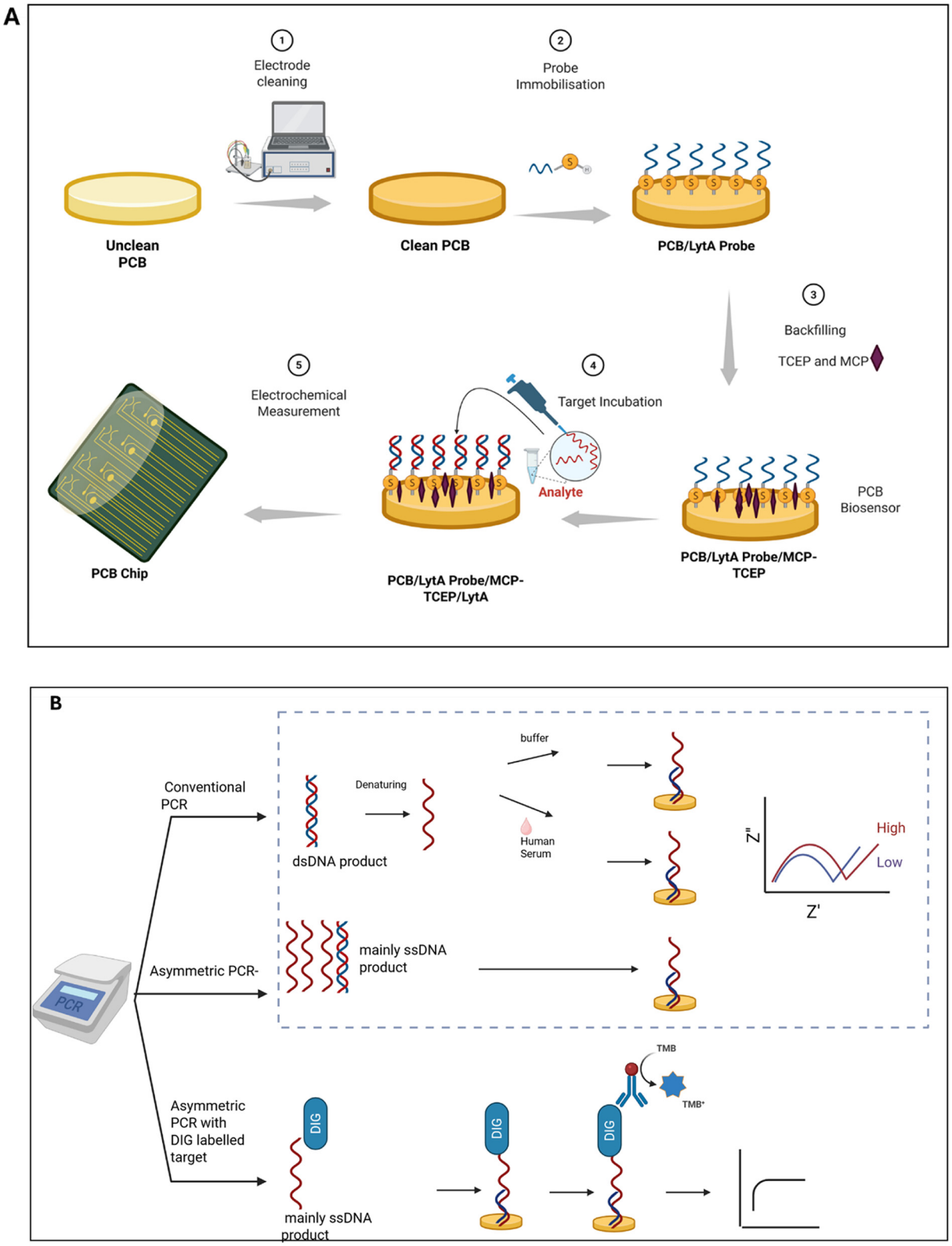

Fig. 2 A) Biosensor fabrication scheme and sensor working principles: (1) electrode cleaning, (2) probe immobilisation, (3) MCP backfilling, (4) target immobilisation, (5) electrochemical measurements using PCB biosensors. B) Amplification procedures used in this work: conventional PCR, asymmetric PCR, and asymmetric PCR with the DIG-labelled target.

by heating at 95 °C for 5 min to convert the double-stranded DNA into single strands. The denatured amplicons were then spiked into 100% human serum (origin: human male AB plasma, USA; sterile filtered, Sigma-Aldrich) to make various target concentrations. Each concentration was sequentially incubated on the electrodes for 15 min at room temperature. After each incubation, the electrodes were washed with 0.05% Tween solution, tested, and then rinsed with PBS before proceeding to the next target concentration. This process was repeated until all concentrations had been tested.

2.7. Electrochemical measurements

Electrochemical measurements were performed using a PalmSens4 potentiostat running with PSTrace software (Alvatek Electrochemical Solutions, Houten, The Netherlands). All measurements in this work were performed sequentially on individual working electrodes using an MUX8-R2 multiplexer. Measurements were performed in at least triplicate, and the averaged results were used for data analysis and calculations. Each PCB electrode utilised its inbuilt Au counter and reference electrodes. Unless otherwise specified in the figure captions, the redox buffer used for all measurements consisted of 2.0 mM $K_3Fe(CN)_6$ and 2.0 mM $K_4Fe(CN)_6$ prepared in 0.5× PBS. The measurement parameters for chronoamperometry (TMB-based): applied potential (E_{dc}) = −0.15 V; duration = 2 s. Electrochemical impedance spectroscopy (EIS) parameters: DC bias potential = 0.0 V (*vs.* open-circuit potential); frequency range = 1 Hz to 50 kHz.

3. Results and discussion

3.1. Designing PCBs

The first PCB designed in this work was designated PCB P1. It consisted of eight working electrodes of various diameters (Table S1), arranged around a central circular reference electrode and an annular counter electrode (Fig. 1A), and was manufactured in-house. The objectives for this prototype were (1) to assess whether the copper pads and traces could be successfully plated with gold, (2) to evaluate the ease and speed of interfacing the PCB with a potentiostat measurement system, and (3) to determine whether the Au surface is capable of providing suitable electrochemical responses that would justify further development for biosensing applications.[21,22] PCB P1 incorporates multiple working electrodes with different diameters as part of a geometry exploration study. All working electrodes were used, they were just normalised by their area to make them comparable, and no mixing of data from different diameters occurred within a given analysis. When comparisons were made across different working electrode geometries, current density and area-normalised impedance were used to ensure that the results were normalised to electrode area and therefore directly comparable despite geometric differences.

Next, commercially manufactured PCBs were purchased. The design was changed to include eight working electrodes of equal diameter and rectangular reference and counter electrodes, generating a more spatially efficient layout (Table S1). Two versions of this updated design were obtained: (1) PCB P2, which was Au plated by the manufacturer, and (2) PCB P3, which was left non-plated to allow for in-lab testing of various Au plating techniques. Utilising a third-party manufacturer enabled the production of a larger number of devices and better quality of fabrication. Both PCBs P2 and P3 exhibited electrochemical responses characteristic of Au surfaces. Notably, PCB P3 demonstrated superior electrochemical behaviour, although with limited reproducibility. Drawing from the insights gained through the development and testing of PCBs P1 to P3, a refined version was designed and commercially produced. This final electrode, offering optimal and reproducible performance, was designated as PCB P4.

Thus, the four PCB electrodes were selected to represent a progression of fabrication pathways relevant to biosensor development and scale-up: from in-house prototyping (P1) to commercial manufacturing with varying levels of optimization (P2–P4). Their surfaces are inherently dissimilar due to differences in manufacturing processes, which directly influence surface properties such as roughness and active area. This variability allows for a practical comparison of how common fabrication choices impact electrochemical biosensing performance when tested under identical assay conditions. The goal of this comparison was to identify the manufacturing route that provides the optimal balance of sensitivity, reproducibility, and scalability for a low-cost diagnostic platform.

3.2. *lytA* detection using custom PCB electrodes

The *lytA* DNA detection performance of the four PCB designs (P1–P4) was evaluated using differential pulse voltammetry (DPV) and EIS. All electrodes underwent identical self-assembled monolayer (SAM) functionalization, with measurements conducted in 5.0 mM redox buffer. DPV measurements were performed on all four PCB designs before and after incubation with 500 pM *lytA* target DNA. Fig. 3A presents the DPV current densities, while Fig. 3B shows the corresponding baseline-subtracted currents. PCB P1 exhibited a moderate current decrease (−44%) upon 1.0 nM *lytA* addition, though the target and control groups overlapped, indicating no significant differentiation. PCB P2 showed a 41.5% current increase at 1.0 μM *lytA* but similarly lacked statistical distinction from the SAM group. In contrast, PCB P3 demonstrated a pronounced current reduction (≈95%) at 500 pM *lytA*, with clear separation between target and control data without any overlap. However, it suffered from electrode loss (4 electrodes) and inconsistent performance. PCB P4

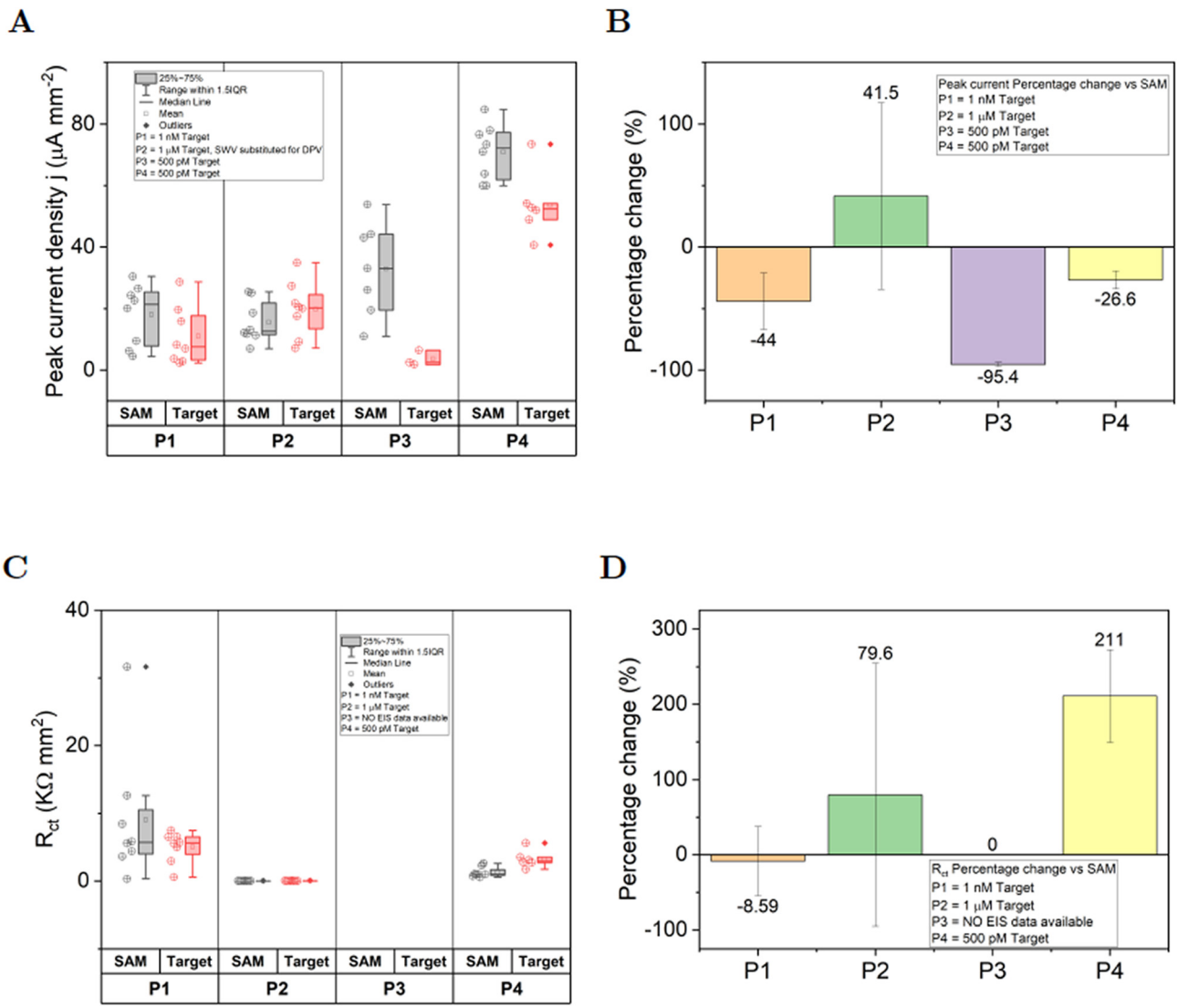

Fig. 3 Performance comparison of four PCB designs (P1–P4) for *lytA* detection. (A) DPV current density for each PCB electrode after SAM formation (control) and after incubation with 500 pM *lytA* target DNA and (B) corresponding percentage change in DPV peak current for each PCB type upon target addition. (C) Charge transfer resistance (R_{ct}) values from EIS measurements for each PCB after SAM formation and after incubation with 500 pM lytA target and (D) corresponding percentage change in R_{ct} for each PCB type upon target addition. All measurements were performed in 5.0 mM redox buffer. Data points represent individual replicates (n = 8).

also displayed significant current decreases (≈26%) at 500 pM, with compacted distributions and no data overlap between groups. Two outliers were observed, but their inclusion did not alter the conclusion of distinct target/SAM responses. Notably, P4 initially lost two electrodes due to a connector issue (unrelated to the electrodes themselves), which was resolved in subsequent experiments. Fig. 3C presents the charge transfer resistance (R_{ct}) values from EIS measurements before and after incubation with 500 pM *lytA* target DNA addition for each PCB electrode, and Fig. 3D presents the corresponding percentage changes. PCB P1 showed a minor R_{ct} decrease reduction (−8.6%), with overlapping distributions indicating no significant difference. PCB P2 exhibited minimal impedance values and a 76.6% increase, though not discernible from DPV data due to axis scaling; no statistical distinction was found. P3 produced unreliable EIS fits, precluding analysis. In contrast, PCB P4 demonstrated a clear 211% increase in impedance, with non-overlapping data ranges suggesting reliable target detection.

Overall, PCBs P1 and P2 failed to demonstrate reliable *lytA* detection. PCB P3 showed promising DPV performance but suffered from inconsistent EIS results and electrode loss. PCB P4 outperformed all other designs, offering robust and reproducible detection of 500 pM *lytA* using both DPV and EIS, with improved electrode consistency following connector repair. Based on its superior sensing performance, stability, and reliability, PCB P4 was selected for all subsequent biosensing experiments.

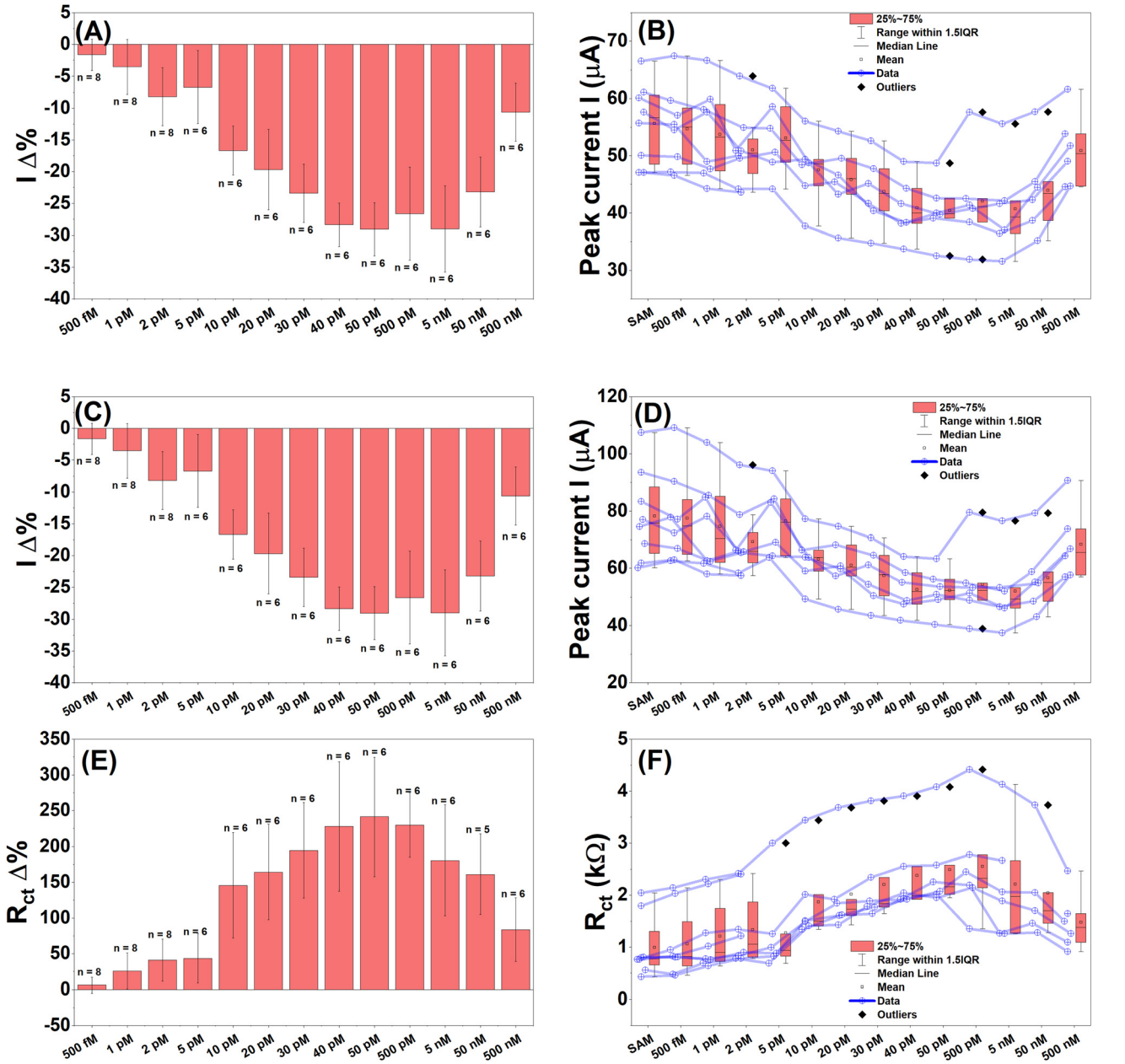

Fig. 4 Concentration-dependent detection of the 20 bp *lytA* target using PCB P4. (A) Mean percentage change in DPV peak current across target concentrations (500 fM to 500 nM) and (B) corresponding raw DPV peak current values at each concentration. (C) Mean percentage change in SWV peak current across different target concentrations (500 fM to 500 nM) and (D) corresponding raw SWV peak current values at each concentration. (E) Mean percentage change in R_{ct} from EIS measurements and (F) corresponding raw R_{ct} values at each concentration. All measurements were performed in 5.0 mM redox buffer. Sample size n = 5–8.

3.3. Detailed investigation of *lytA* detection using PCB P4

The performance of PCB P4 for detecting various concentrations of *lytA* target DNA was evaluated, and the results are presented in Fig. 4. The DPV response current linearly decreased and showed a dose-dependent fashion for different target concentration ranges from 500 fM to 500 nM. The mean percentage change in DPV peak current demonstrated a generally linear and dose-dependent decrease in response to increasing *lytA* concentrations. However, the 5.0 pM concentration slightly deviated from this trend, and a trend reversal was observed at 50 pM, after which the signal continued to decrease with higher concentrations (Fig. 4A). This unexpected trend reversal most likely occurred due to the multiple incubation, washing and testing processes, destabilising the probe DNA. The corresponding raw DPV peak current data showed considerable spread, with significant differences likely occurring between the SAM control and the 30 pM to 50 nM target concentrations; the remaining concentrations appeared statistically similar

(Fig. 4B). Square wave voltammetry (SWV) results exhibited comparable percentage change magnitudes and dose–response trends across a range of 500 fM to 500 nM (Fig. 4C), with the raw data reflecting similar behaviour to DPV but with fewer outliers (Fig. 4D). Likely significant differences between the SAM control and target samples were again observed in the 30 pM to 50 nM range. The mean R_{ct} percentage change from the EIS results also showed a dose-dependent increase, with the 5.0 pM concentration again deviating from the overall trend and with a noticeable reversal at 50 pM, consistent with the DPV and SWV results (Fig. 4E). Notably, the magnitude of the EIS response was significantly larger, about 250% compared to the ~30% observed with DPV and SWV. The raw R_{ct} data showed several outliers; exclusion of these would have reduced the magnitude of the percentage change but improved statistical errors (Fig. 4F). Significant differences between the SAM control and the target DNA were evident from 10 pM up to 50 nM. Overall, EIS was found to be the best performing detection technique among the CV, SWV and EIS, demonstrating the highest magnitude of percentage changes, clearer distinctions between control and target stages, and smaller data spreads for each concentration of *lytA*.

Further analysis of *lytA* detection performance on PCB P4 was conducted by performing linear regression within the linear response region between 10 pM and 50 pM. The LoD was also calculated. The LoD for *lytA* was determined to be 10.4 pM, 12.39 pM, and 4.5 pM using DPV, SWV, and EIS, respectively. A second linear response region was observed in all three techniques, between 0 and 2.0 pM, yielding LOD values ranging from 251 to 433 fM. This suggests that the PCB P4 biosensor is capable of detecting femtomolar concentrations of 20 bp complementary *S. pneumoniae* DNA, indicating potential for ultra-sensitive detection. Notably, a previously reported peptide nucleic acid (PNA)-based PCB device for rapid and high-sensitivity DNA quantification reported an LoD of 57 fM.[17] The biosensor described in this work demonstrated comparable LoDs (251–433 fM) without requiring expensive PNA reagents, instead relying on a straightforward SAM modification strategy.

3.4. PCR amplification of genetic sequences at PCB P4

With a suitable platform established and successful detection of the 20 bp complementary *lytA* DNA sequences in PBS, the performance of the probe was next subjected to longer DNA target fragments. This aimed to more precisely replicate the DNA lengths that a sensor would be required to deal with in PoC settings. For this purpose, a 235 bp sequence (amplified from *S. pneumoniae* genomic DNA) that contained 20 bp *lytA* complementary sequence in the middle of the larger sequence was used. The reason for it being in the middle and not at the ends of the sequence was due to the primer design from the previous literature.[19] To further validate the specificity of the *lytA* probe, negative controls were included using 115 bp oxa amplicons.

Table 2 List of PCR amplifications

S. no.	Amplifying target	Length (bp)	Qubit quantification (μg mL^{-1})
1.	*lytA* (*S. pneumoniae*)		
	Positive	235	14.1
	Negative	NA	0.9
2.	*lytA* (*S. pneumoniae*) DIG		
	Positive	235	3.29
	Negative	NA	2.57
3.	*lytA* (*S. pneumoniae*) asymmetric		
	Positive	235	6.73
	Negative	NA	0.399
4.	*lytA* (*S. pneumoniae*) asymmetric DIG		
	Positive	235	8.73
	Negative	NA	1.11
5.	Oxa (*E. coli*)		
	Positive	115	11.3
	Negative	NA	2.78
6.	Oxa (*E. coli*) DIG		
	Positive	115	4.89
	Negative	NA	2.75
7.	Oxa (*E. coli*) asymmetric		
	Positive	115	5.13
	Negative	NA	2.16
8.	Oxa (*E. coli*) asymmetric DIG		
	Positive	115	46.4
	Negative	NA	2.23

3.4.1. *lytA* 235 bp and oxa 115 bp PCR amplification. The PCR amplification of the 235 bp *lytA* target was first assessed using a Qubit 4 fluorometer, and the results are given in Table 2. The positive amplified *lytA* PCR mixture yielded a concentration of 14.1 μg mL^{-1}, while the negative control (without genomic DNA template) showed only 0.9 μg mL^{-1}. This clear difference confirmed successful amplification in the positive sample. This quantification confirmed the presence of amplified nucleic acid but could not verify whether it was the desired *lytA* DNA sequence. To confirm the specificity of the amplification, gel electrophoresis was performed on both positive and negative PCR products (Fig. S3A). The negative control showed no visible band, indicating that no significant amplification occurred. In contrast, a visible band in the positive lane was observed between the 200 and 300 bp on the reference ladder, confirming the amplification of a product consistent with the desired 235 bp *lytA* amplicon.

Similarly, for the oxa amplifications, the positive PCR mixture showed a concentration of 11.3 μg mL^{-1}, while the negative control measured 2.78 μg mL^{-1} (Table 2). The significantly higher concentration in the positive sample confirmed successful nucleic acid amplification. The gel electrophoresis analysis revealed no visible band in the negative lane, while the positive lane showed a clear band in the lower end in the range of 100–200 bp (Fig. S3B), consistent with the desired sequence of 115 bp long amplicon. The distorted appearance of the gel was noted,

which could be attributed to water vapour condensation on the plastic cover. These results confirmed successful amplification of the oxa amplicons, enabling the subsequent specificity testing.

3.4.2. Asymmetric and asymmetric DIG-labelled *lytA* and OXA PCR amplification. The PCR amplifications of DIG-labelled *lytA* and oxa, as well as asymmetric oxa, did not attain successful quantification results (Table 2). Positive samples showed relatively lower concentrations, while negative controls showed higher values. However, asymmetric DIG-labelled oxa displayed notably high amplification (46.4 μg mL^{-1}), with its corresponding negative showing a low concentration, indicating successful amplification. Gel electrophoresis of these samples revealed that all *lytA* samples (both DIG-labelled and unlabelled) failed to show bands in either the positive or negative lanes (Fig. S3C). DIG-labelled oxa showed bands in both the positive and negative lanes, indicating possible contamination in the negative control. Asymmetric oxa showed no visible bands, while asymmetric DIG-labelled oxa displayed a band in the positive

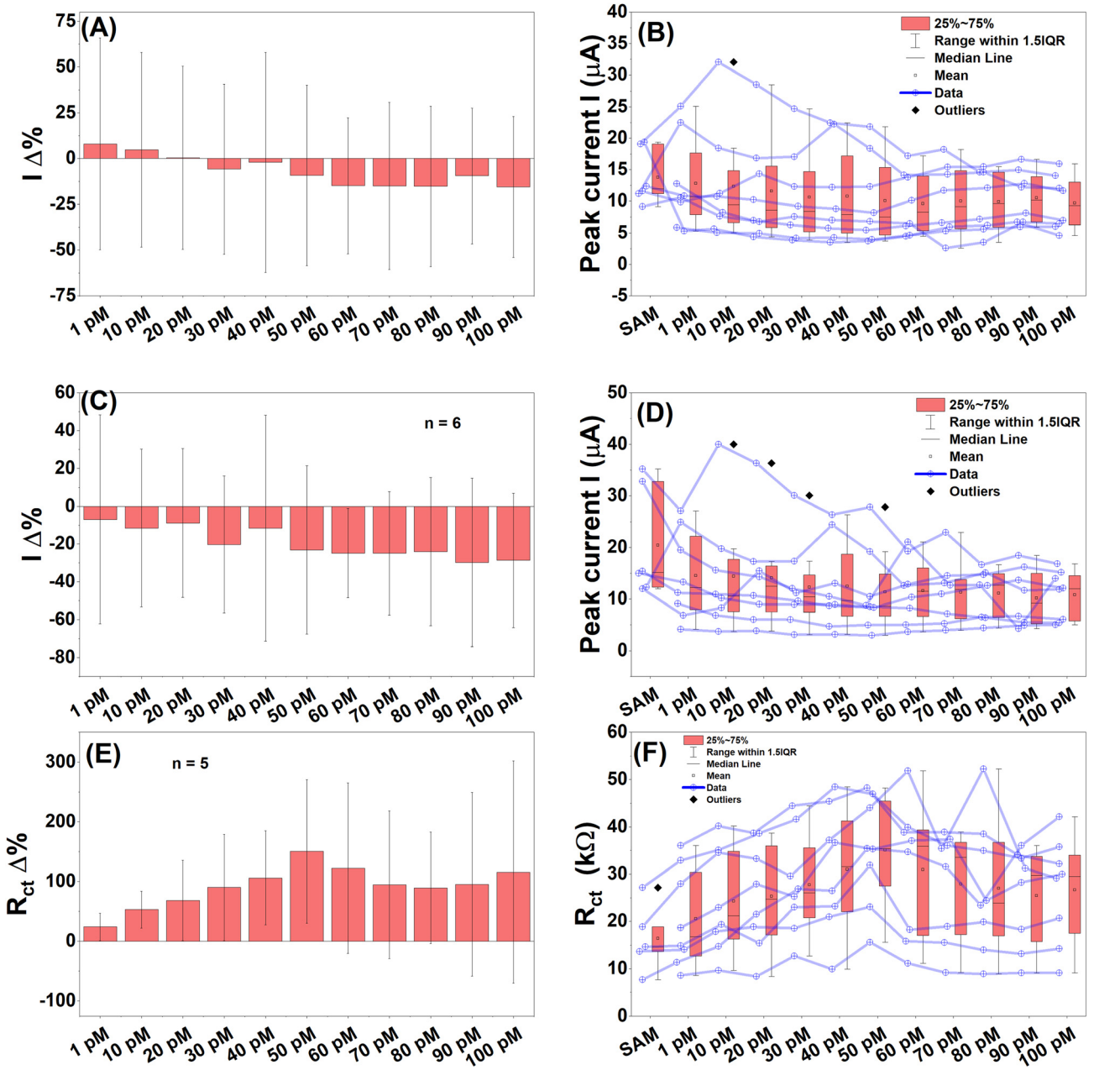

Fig. 5 Detection of *lytA* 235 bp PCR amplicons in PBS using PCB P4. (A) Mean percentage change in DPV peak current for target concentrations ranging from 1.0 pM to 100 pM and (B) corresponding raw DPV peak current values. (C) Mean percentage change in SWV peak current for various target concentrations and (D) corresponding raw SWV peak current values. (E) Mean percentage change in R_{ct} from EIS measurement for various target concentrations. (F) Corresponding raw R_{ct} values. All measurements were conducted using a ferri/ferrocyanide redox buffer. n = 8.

lane but not in the negative lane. The inconsistent behaviour observed in the gel, particularly the presence or absence of bands, may have resulted from pipetting errors or sample misloading, leading to inconclusive electrophoresis outcomes. Despite the inconclusive gel results, Qubit quantification indicated the likely presence of amplicons in several of these samples. Therefore, experiments using these PCR products proceeded, with subsequent biosensing results potentially serving to validate the success of the amplifications.

3.5. *lytA* genetic amplicons in PBS using PCB P4

3.5.1. Detection of 235 bp *lytA* amplicons in PBS. The 235 bp *lytA* amplicon was diluted in PBS to prepare a range of target concentrations (1.0 pM to 100 pM). Prior to electrode incubation, the DNA solutions were denatured at 95 °C for 5 min to ensure single-stranded DNA, then transferred to the electrode surfaces and incubated for 15 min. Although the mean DPV percentage change initially increased with target concentration, it subsequently showed a gradual decline

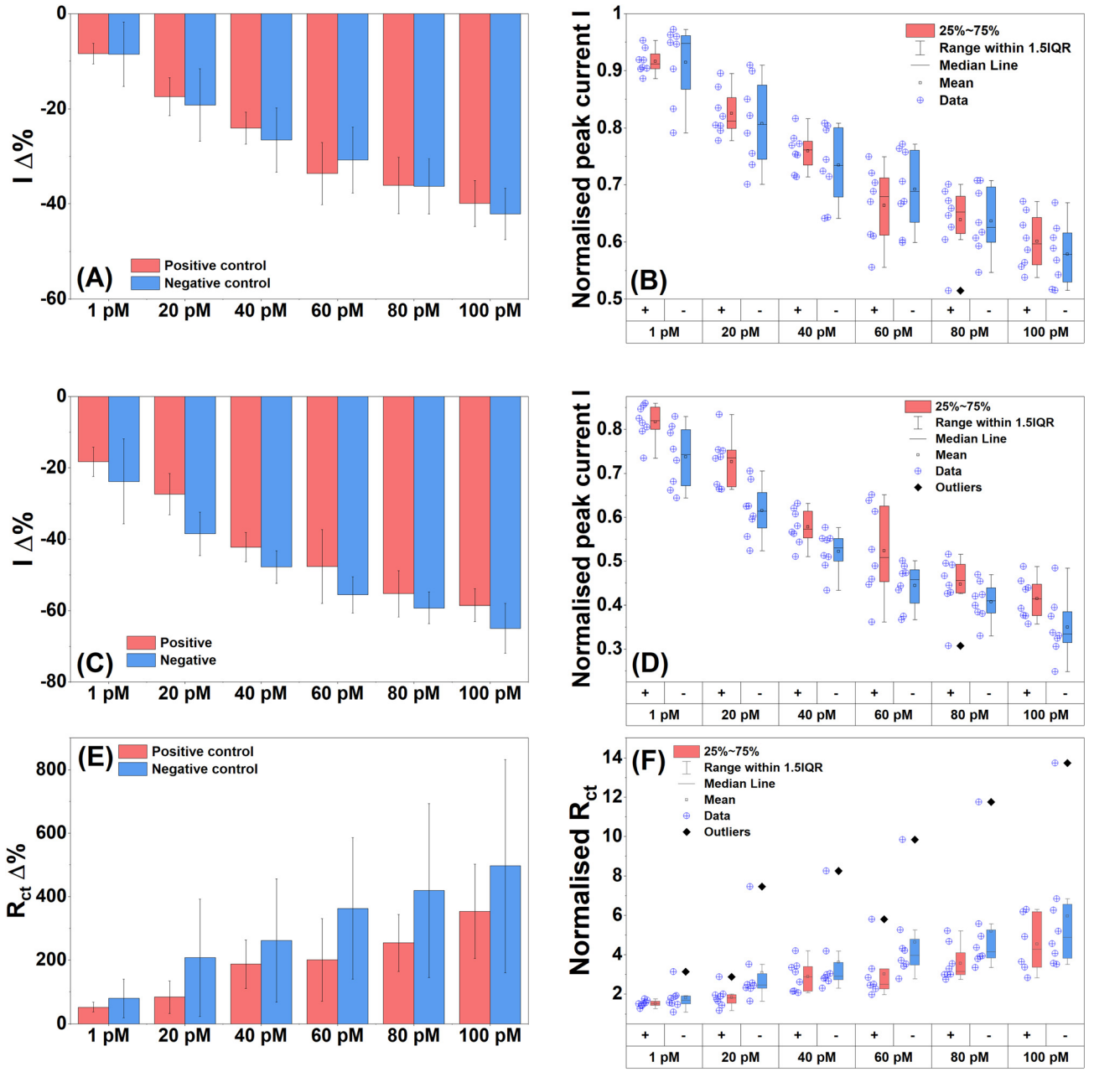

Fig. 6 Detection of asymmetric *lytA* 235 bp amplicons in PBS using PCB P4. (A) Mean percentage change in DPV peak current for target concentrations ranging from 1.0 pM to 100 pM and (B) corresponding raw DPV peak current values. (C) Mean percentage change in SWV peak current across various target concentrations (1.0 pM to 100 pM) and (D) corresponding raw SWV peak current values. (E) Mean percentage change in R_{ct} from EIS measurements for various target concentrations (1.0 pM to 100 pM) and (F) corresponding raw R_{ct} data. n = 8.

(Fig. 5A). However, no clear dose-dependent trend was observed, and the results were marked by overlapping error bars. The raw DPV current data confirmed this, showing no statistically significant differences between the control and target stages (Fig. 5B). Similar results were observed with SWV for the same concentration range (1.0 pM to 100 pM), where the percentage changes lacked a clear dose response and were accompanied by overlapping errors (Fig. 5C). The initial response was found to decrease, however, contrary to the DPV behaviour, remained that way for all target concentrations. There appeared to be an absence of differences between SAM and target stages, with the introduction of more outliers (Fig. 5D). EIS delivered the most promising results. The mean R_{ct} percentage change showed a dose-dependent increase from 1.0 pM to 50 pM, with a trend reversal phenomenon appearing again at 50 pM (Fig. 5E). Although the R_{ct} data for the target stages exhibited wide variability, the SAM stage had a narrower spread, enabling likely differentiation between the SAM and target stages in the 20–50 pM range (Fig. 5F). These EIS results confirmed the successful detection of the 235 bp *lytA* amplicons in PBS using the PCB P4 electrode.

3.5.2. Asymmetric *lytA* and oxa amplicons in PBS. The asymmetric PCR amplicons were incubated on separate PCBs (positive and negative) for 15 min in PBS. Heating was not required, as the asymmetric reaction is expected to produce single-stranded DNA directly suitable for sensor interaction. The mean DPV percentage changes displayed a decreasing dose-dependent response with increasing concentrations of the positive (*lytA*) amplicon target from 1.0 pM to 100 pM (Fig. 6A). The negative control (oxa) also showed a dose-dependent response and produced a slightly higher response than the positive. The normalised DPV data confirmed the absence of statistically significant differences between the *lytA* and oxa responses (Fig. 6B), though the data spread and associated errors were improved compared to the first amplicon experiment. The SWV response was similar to DPV results, showing comparable dose responses for both control groups (Fig. 6C), but with a greater magnitude of percentage change. Notably, potential significant differences between the positive and negative groups were observed at 20 pM and 40 pM (Fig. 6D), suggesting that the negative amplicon generated a stronger response than the positive, which was an unexpected result. EIS results also revealed dose-dependent trends in both control groups, with the negative showing a greater response overall (Fig. 6E). The data were affected by large errors in some stages, particularly in the positive and most negative conditions. Normalised R_{ct} data indicated that these large variances could largely be attributed to a single outlier electrode; when excluded, the data showed potential significant differences at 20 pM and 60 pM (Fig. 6F). However, the outlier was retained in the percentage change data for full transparency, serving as a reminder that improved error margins could be achieved by statistically rejecting such anomalous data points.

These results can likely be attributed to non-specific biofouling of the electrode surface. As shown in Table 2, both asymmetric *lytA* and oxa reactions produced similar levels of amplified materials (6.73 and 5.13 μg mL^{-1}, respectively). However, the gel electrophoresis analysis for both showed no indication of bands in their lanes which suggested that the specific DNA material was not present in the sample. If this were true, then both PCBs exposed to the *lytA* positive and oxa negative were in reality receiving various concentrations of non-specific proteins and nucleotide mixtures that composed the PCR solutions. The responses seen here would then easily be explained as a biofouling dose response of these protein/nucleotide contaminants with none or insufficient quantities of amplicons present.

3.5.3. Asymmetric DIG-labelled *lytA* and oxa amplicons in PBS. About 40 pM positive and negative amplicons were incubated on the electrodes for 15 min at 50 °C, followed by washing and subsequent incubation with HRP tagged anti-DIG antibodies at room temperature for 30 min. The mean DPV percentage change showed that both controls had decreased current change (Fig. S4A). The positive decreased more than the negative −40% *vs.* −10%. The normalised DPV peak currents confirmed this behaviour resulting in a likely difference between the controls demonstrating successful specific detection of 40 pM asymmetric DIG-labelled *lytA* DNA (Fig. S4B). The mean R_{ct} percentage change showed an increase in response target 100% *vs.* 40% (Fig. S4C). The normalised R_{ct} data supported this and was on the verge of a likely difference (Fig. S4D).

The PCBs were washed after the previous measurements and TMB was applied for 20 min. The TMB solution turned blue confirming the presence of HRP. Chronoamperometry was performed producing a current decrease for both positive and negative controls (Fig. 6 and S4E, test 1). There were no differences between the controls. To ensure that the unspecifically bound HRP was properly removed, a second washing step incorporating 20 s of 1× PBS, 20 s of 0.05% Tween, and then 20 s of 0.1× PBS was performed and reapplication of TMB for 20 min was undertaken. The response again showed a current decrease for both controls with the negative decreasing more than the positive (Fig. S4E and test 2) producing no differences between the groups. This chronoamperometry method produced TMB colour reactions for both control group solutions when only the positive control should. This meant that the HRP anti DIG antibodies were present on the negative control and were unspecifically bound, with multiple washing attempts unable to successfully remove them.

3.6. *lytA* genetic amplicon in human serum

With successful specific detection of full complementary 20 bp and 235 bp normal PCR and asymmetric DIG-labelled amplicons in PBS, the next step was to attempt detection of the 235 bp amplicon (amplified from *S. pneumoniae* genomic DNA) in a clinically relevant matrix. Normal 235 bp *lytA* and

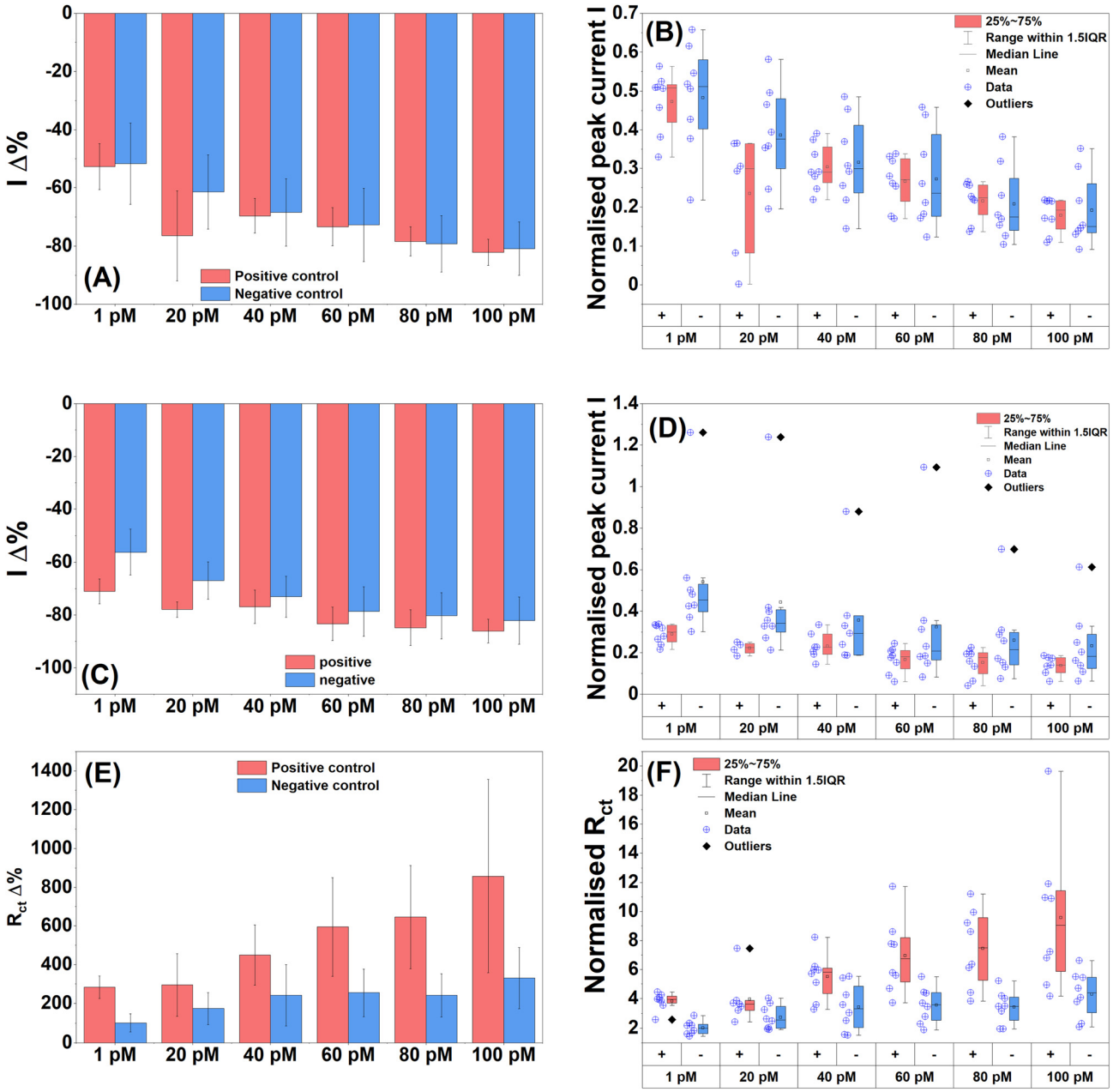

Fig. 7 Detection of PCR amplicons in 100% human serum (*lytA* 235 bp (positive control) *vs.* oxa 115 bp (negative control)) using PCB P4. (A) Mean percentage change in DPV peak current for *lytA* (235 bp) and oxa (115 bp, negative control) targets across a concentration range of 1.0 pM to 100 pM and (B) corresponding normalised DPV current values. (C) Mean percentage change in SWV peak current for *lytA* and oxa over a concentration range of 1.0 pM to 100 pM and (D) corresponding normalised SWV current values. (E) Mean percentage change in R_{ct} from EIS measurements for different concentrations of positive and negative controls over a range of 1.0 pM to 100 pM and (F) corresponding normalised R_{ct} values. All measurements were conducted in 2.0 mM ferri/ferrocyanide redox buffer. n = 8.

115 bp oxa PCR products were heated to 95 °C for 5 min and then spiked into 100% human serum. The serum samples were incubated on the electrode surface for 15 min, Tween washed and then tested. The target concentration range was 1.0 pM to 100 pM. The mean DPV peak current percentage change displayed a dose-dependent response to increasing target with 20 pM failing to follow the trend (Fig. 7A). The negative control also showed a dose-dependent response. The normalised DPV data confirmed the percentage changes with the 20 pM verging on a likely difference between the two controls (Fig. 7B). The other target concentrations showed no differences. The mean SWV peak current percentage changes showed a slight improvement over DPV with more pronounced differences between the control groups (Fig. 7C). Dose dependence was again present for both control groups. The normalised data showed that 1.0 and 20 pM control groups were likely different and 60, 80 and 100 pM were close to being different (Fig. 7D).

Table 3 Table of comparisons of *S pneumoniae* sensors

Sensor/technology	Label free?	Approx. cost per test	Key complexity	LOD (pM)	Time to result	Real sample
Cell culture	Yes	Low	Simple (but slow)	NA	72 h	Blood
PCR	Yes	High	Moderate	NA	Hours	Extracted DNA
UAT[30]	Yes	≈£5	Moderate	NA	15 min	Urine
Magnetosensor[19]	No	High (~£4.65)	High (MB modification)	1100	5 h	Buffer
DNA antibody[23]	No	Very high	Very high (DNA tetrahedron)	3.26	>30 min	Serum
Polymer genosensor[24]	Yes	High	Moderate	1×10^6	20 min @ 55 °C	Buffer
Synergism gene sequence[25]	No	Very high	High (multiple probes)	0.0005	20–60 min	50% serum
LAMP[26]	No	Moderate (≈£2.80)	High (microfluidics)	0.173	≈2 h	Clinical samples
PNA-based lab-on-PCB[17]	Yes	Moderate (PNA costly)	High (microfluidics)	0.057	5 min (flow)	Buffer
PCB electrodes (this work)	**Yes**	**Very low (≈£0.2)**	**Low (standard SAM)**	**1.0**	**15 min**	**100% serum**

Abbreviations: UAT: urinary antigen test; LAMP: loop-mediated isothermal amplification; PNA: peptide nucleic acid; MB = magnetic beads.

EIS again proved to be the best performing detection technique with the PCB P4 biosensor. The mean R_{ct} percentage change showed increasing dose dependence for the positive control (Fig. 7E). The negative control increased until 40 pM and then remained constant until 100 pM where it then increased slightly. Therefore, the negative control did not produce a strong dose response, and the sensor demonstrated anti-biofouling properties. The normalised mean R_{ct} data showed likely differences between positive and negative groups for 1.0, 60, 80 and 100 pM (Fig. 7F). Some positive target stages were likely different from each other indicating a strong signal response to target DNA while no differences were found within the negative control groups, meaning that they were all likely equivalent further reinforcing the anti-biofouling performance of the sensor. The LoD values for the various measurement techniques were calculated, which were 23 pM for DPV, 30 pM for SWV, and 18 pM for EIS. The LoD values correlated with the concentrations demonstrated to have likely differences from the box plot data, with the exception of EIS which was able to successfully detect target DNA at 1.0 pM which was significantly lower than the calculated LoD.

Table 3 summarises the comparisons with sensors from the literature. Compared to several previous sensors, the developed sensor demonstrated excellent responses for such a simple device and would hopefully continue showing such responses with testing of reduced concentrations and incubation times. This is a vast improvement on current culture methods which regularly return no culture positive after multiple hours of incubation. This sensor also outperforms the pneumococcal urinary antigen test in terms of time to result, expense and complexity. The time to result values are both 15 min but this should be easily reduced on this sensor system. The sensor does not require to be at specific temperature nor do the sample and reagents.[11] This sensor comprises sample addition, washing, redox addition and then results, reducing the complexity of the assay. The antigen test requires samples and multiple reagents. Antigen tests are relatively expensive approximately in £3–£5, whereas this sensor would likely be in the region of pence if it aligns its manufacture protocol with that of glucose strip production which is demonstrated in the next section for a Coronavirus Disease 2019 (COVID-19) sensor. Other tests on the market include a magnetogenosensor assay for *lytA* that was able to obtain a LoD of 1100 pM.[19] Other examples of reported *S. pneumoniae* sensors include a DNA–antibody nanostructure assay (≈3.26 pM),[23] a polymer-based genosensor (≈1×10^6 pM),[24] a synergism strategy for gene sequence sensing (0.0005 pM),[25] and versatile loop-mediated isothermal amplification with a sensitivity of 0.173 pM.[26] The sensor developed in this work demonstrated similar or improved sensitivity to the devices reported. It was also able to achieve this in complex human serum with reduced time to result utilising less complicated functionalisation strategies on an easily manufacturable device. The sensors above that demonstrate low pM detection used complex devices, materials and methods to achieve this. The PCB P4 design, which provides a dedicated counter and reference electrode for each working electrode, creates an array of independent electrochemical cells. This design inherently minimizes the risk of crosstalk, a significant advantage for future parallelized operation in a point-of-care device.

For deployment as a practical PoC device, this PCB electrode can be integrated into a single-use, disposable cartridge designed for 'plug-and-play' operation. Our group recently demonstrated a similar plug-and-play, easy-to-manufacture PoC device for diagnostic applications.[27] Such cartridge houses can protect the delicate electrodes and electrical contacts, incorporates a defined sample chamber with a simple injection port for regulated sample introduction, and ensures robust fluidic containment to prevent user exposure to the sample or reagents. The user would simply inject the prepared sample, insert the cartridge into a portable, handheld reader, and receive a digital readout. This approach, common in commercial glucose meters and other POC diagnostics, effectively decouples the complex microfluidics and electrochemistry from the end-user, ensuring reliability, safety, and ease of use. Future work will focus on prototyping such cartridges and integrating them with low-cost, portable readers.

For translation to a field-deployable POC device, power consumption is a key practical consideration. The electrochemical techniques employed (EIS and DPV) require very low operating currents (<100 μA). Commercial mini-

potentiostats demonstrate that such systems can run for extended periods on small batteries or a smartphone connection.[28,29] Therefore, a dedicated reader for this PCB platform would have minimal power demands, easily supporting a full day of operation on a compact, rechargeable battery, aligning with the requirements for use in resource-limited settings.

These results demonstrated that SWV could partially, and EIS could fully successfully and specifically detect an unlabelled 235 bp *lytA* amplicon amplified from *S. pneumoniae* full genomic DNA over a range of concentrations from 1.0–100 pM in 15 min at room temperature. Clinically relevant blood levels that can result in life-threatening infections can be as low as 1–10 colony-forming units per millilitre of blood (cfu mL^{-1}).[31] This equates to approximately attomolar (aM) levels of genetic material for detection. The sensor has shown possible femtomolar LoDs and should comfortably be able to detect these femtomolar concentrations. Attomolar ranges would be a challenge to achieve, nevertheless until the sensor is tested with these concentrations, no feasibility conclusions can be made. If the sensor was unable demonstrate detection at these small concentrations, then PCR amplification would have to be employed to amplify the DNA to detectable levels. This would be easily accomplished as PCR amplification was already employed for target sequence production for these experiments. Therefore, the infrastructure already existed and has been successfully demonstrated. Two hours of amplification was required to produce nanomolar levels of target DNA with the sensor demonstrating picomolar capabilities. Consequently, the attomolar DNA would only require amplification to picomolar levels shortening the current amplification times used. This would result in the successful detection of clinically relevant levels of *S. pneumoniae* in under 2 h.

4. Conclusions

This study systematically investigated PCB-based electrodes for rapid sepsis diagnostics through *S. pneumoniae lytA* DNA detection. While prototype PCBs (P1–P3) showed progressive improvements in electrochemical performance, they faced limitations in reliability and consistency. The commercially fabricated PCB P4 emerged as the optimal platform, demonstrating superior and reproducible DNA detection capabilities, making it ideal for sepsis biosensor development. Using a 20 bp *lytA* sequence, we established a PCB P4-based electrochemical detection system with a 4.5 pM LoD in PBS. The system was further validated with PCR-amplified longer target sequences and successfully detected normal double-stranded DNA amplicons, asymmetric (single-stranded DNA) and asymmetric DIG-labelled amplicons, and 235 bp *lytA* sequences spiked in 100% human serum (1–100 pM detection *via* EIS in 15 min at room temperature). While some asymmetric PCR products showed detection limitations due to potential quantity/contamination issues, the platform demonstrated clinically relevant sensitivity. This work presents a functional biosensor capable of detecting 1.0 pM *lytA* amplicons in complex matrices within 15 minutes at ambient temperature. With further optimization, this system shows strong potential for reduced detection times, enhanced sensitivity, and direct clinical sample analysis. The developed PCB platform establishes a foundation for rapid, point-of-care sepsis diagnostics with significant translational promise.

Conflicts of interest

The authors declare no conflicts of interest.

Data availability

Key data that support the findings of this study have been included in the manuscript. Additional data that support this article have been included as part of the supplementary information (SI). Supplementary information: electrochemical set-up for gold plating and cleaning, procedure for gold plating on PCB electrodes, cleaning of gold PCB electrodes, table for PCB specifications, optimized chemical cleaning and electrochemical procedure, and additional figures. See DOI: https://doi.org/10.1039/d5sd00210a.

Acknowledgements

This work was supported by the Centre for Advanced Measurement Science and Health Translation, University of Strathclyde. PAH would like to acknowledge the Royal Academy of Engineering Research Chair Scheme for long term personal research support (RCSRF2021\11\15). DA would like to acknowledge educational support from Baxter Pharmaceuticals and MSD (Merck Sharp and Dohme). DC would like to thank the Dowager Countess Eleanor Peel Trust and Tenovus Scotland for seed grants in the area of sepsis monitoring. VV's EngD studentship was funded by the EPSRC CDT in Biomedical Devices and Health Technologies (EP/L015595/1).

References

1 J.-L. Vincent, *EBioMedicine*, 2022, **86**, 104318.
2 T. K. Burki, *Lancet Respir. Med.*, 2018, **6**, 826.
3 C. F. Duncan, T. Youngstein, M. D. Kirrane and D. O. Lonsdale, *Curr. Infect. Dis. Rep.*, 2021, **23**, 1–14.
4 I. Martin-Loeches, L. F. Reyes and A. Rodriguez, *Thorax*, 2025, **80**, 565–575.
5 N. Gopal, N. Chauhan, U. Jain, S. K. Dass, H. S. Sharma and R. Chandra, *Artif. Cells, Nanomed., Biotechnol.*, 2023, **51**, 476–490.
6 A. S. Tanak, A. Sardesai, S. Muthukumar and S. Prasad, *Bioeng. Transl. Med.*, 2022, **7**, e10310.
7 S. Balayan, N. Chauhan, R. Chandra, N. K. Kuchhal and U. Jain, *Biosens. Bioelectron.*, 2020, **169**, 112552.

8 R. Varghese, R. Jayaraman and B. Veeraraghavan, *J. Microbiol. Methods*, 2017, **141**, 48–54.
9 S. L. Goh, B. P. Kee, K. Abdul Jabar, K. H. Chua, A. M. Nathan, J. Bruyne, S. T. Ngoi and C. S. J. Teh, *Pathog. Global Health*, 2020, **114**, 46–54.
10 W.-T. Fan, T.-T. Qin, R.-R. Bi, H.-Q. Kang, P. Ma and B. Gu, *Eur. J. Clin. Microbiol. Infect. Dis.*, 2017, **36**, 1005–1012.
11 P. Kim, A. Deshpande and M. B. Rothberg, *Infect. Drug Resist.*, 2022, 2219–2228.
12 B. Kim, J. Kim, Y. H. Jo, J. H. Lee, J. E. Hwang, M. J. Park and S. Lee, *PLoS One*, 2018, **13**, e0200620.
13 P. Lasserre, B. Balansethupathy, V. J. Vezza, A. Butterworth, A. Macdonald, E. O. Blair, L. McAteer, S. Hannah, A. C. Ward and P. A. Hoskisson, *Anal. Chem.*, 2022, **94**, 2126–2133.
14 S. Kumar, S. Tripathy, A. Jyoti and S. G. Singh, *Biosens. Bioelectron.*, 2019, **124**, 205–215.
15 S. Mahapatra, R. Kumari and P. Chandra, *Trends Biotechnol.*, 2024, **42**, 591–611.
16 H. Shamkhalichenar, C. J. Bueche and J.-W. Choi, *Biosensors*, 2020, **10**, 159.
17 P. Jolly, J. Rainbow, A. Regoutz, P. Estrela and D. Moschou, *Biosens. Bioelectron.*, 2019, **123**, 244–250.
18 D. Llull, R. Lpez and E. Garca, *J. Clin. Microbiol.*, 2006, **44**, 1250–1256.
19 S. Campuzano, M. Pedrero, J. L. Garca, E. Garca, P. Garca and J. M. Pingarrn, *Anal. Bioanal. Chem.*, 2011, **399**, 2413–2420.
20 N. Woodford, A. Carattoli, E. Karisik, A. Underwood, M. J. Ellington and D. M. Livermore, *Antimicrob. Agents Chemother.*, 2009, **53**, 4472–4482.
21 D. Pletcher, *A first course in electrode processes*, Royal Society of Chemistry, 2009.
22 R. G. Compton and C. E. Banks, *Understanding voltammetry*, World Scientific, 2007.
23 J. Wang, M. C. Leong, E. Z. W. Leong, W. S. Kuan and D. T. Leong, *Anal. Chem.*, 2017, **89**, 6900–6906.
24 F. P. Ferreira, A. C. Honorato-Castro, J. V. da Silva, S.-C. Orellana, G. C. Oliveira, J. M. Madurro and A. G. Brito-Madurro, *Polym. Eng. Sci.*, 2018, **58**, 1308–1314.
25 F. Li, Z. Yu, Y. Xu, H. Ma, G. Zhang, Y. Song, H. Yan and X. He, *Anal. Chim. Acta*, 2015, **886**, 175–181.
26 H. Wang, Z. Ma, J. Qin, Z. Shen, Q. Liu, X. Chen, H. Wang, Z. An, W. Liu and M. Li, *Biosens. Bioelectron.*, 2019, **126**, 373–380.
27 A. Dobrea, N. Hall, S. Milne, D. K. Corrigan and M. Jimenez, *Sci. Rep.*, 2024, **14**, 14154.
28 A. Ainla, M. P. S. Mousavi, M.-N. Tsaloglou, J. Redston, J. G. Bell, M. T. Fernández-Abedul and G. M. Whitesides, *Anal. Chem.*, 2018, **90**, 6240–6246.
29 K. A. Bautista, E. Madsen, S. D. Riegle and J. C. Linnes, *ACS Electrochem.*, 2025, **1**, 386–394.
30 F. Gutirrez, M. Mar, J. C. Rodrguez, A. Ayelo, B. Soldn, L. Cebrin, C. Mirete, G. Royo and A. M. Hidalgo, *Clin. Infect. Dis.*, 2003, **36**, 286–292.
31 S. O. Kelley, *ACS Sens.*, 2017, **2**, 193–197.